Computational Condensed Matter 8 (2016) 31–35

Contents lists available at ScienceDirect

Computational Condensed Matter

journal homepage: http://ees.elsevier.com/cocom/default.asp

A first principle hybrid functional calculation of Tm_{Ge}^{3+}-V_{Ge} defect complexes in germanium

E. Igumbor [a, b, *], R.E. Mapasha [a], Richard Andrew [a], W.E. Meyer [a, **]

[a] Department of Physics, University of Pretoria, Pretoria 0002, South Africa
[b] Department of Mathematics and Physical Sciences, Samuel Adegboyega University, Km 1 Ogwa/Ehor Rd, Ogwa, Edo State, Nigeria

ARTICLE INFO

Article history:
Received 12 January 2016
Received in revised form
12 July 2016
Accepted 14 July 2016
Available online 19 July 2016

Keywords:
Defects
Charge state
Formation energy
Rare earth

ABSTRACT

By means of density functional theory (DFT), using the screened Heyd, Scuseria, and Ernzerhof (HSE06) hybrid functional we present results of the Tm_{Ge}^{3+}-V_{Ge} defect complexes in germanium (Ge). The formation energies of the first (*fnn*), second (*snn*), third (*tnn*) and fourth ($f_t nn$) nearest neighbour configurations of V_{Ge}-V_{Ge} were examined. The charge state transition levels for all these configurations were examined as well. The Tm_{Ge}^{3+}-V_{Ge} complexes were found to have a positive binding energies for the neutral charge state in the *fnn* and $f_t nn$ configurations. The thermodynamic transition levels revealed that the Tm_{Ge}^{3+}-V_{Ge} induced shallow levels in the band gap for the *fnn*, *tnn* and $f_t nn$ configurations and deep level for the *tnn* configuration. The *snn* configuration showed no charge state transition level, the − 2 charge state was stable for all Fermi energies in the band gap. The Tm_{Ge}^{3+}-V_{Ge} displayed evidence of a single donor level $(+1/0)$ and an acceptor level $(-1/-2)$ within the band gap. Charge state controlled metastability was exhibited by the Tm_{Ge}^{3+}-V_{Ge}.

1. Introduction

Study of defects in semiconductor materials have been intensively carried out in the last two decades, most especially for materials such as Si and Ge [1]. While the former has a band gap of 1.11 eV [2], the latter has a narrow band gap of 0.78 eV [3] at 0 K. The high electron and hole mobilities of Ge has made it possible for strained Si_{1-x} Ge_x heterostructures to increase mobility in modern transistors [4]. Impurities influence Ge-based semiconductor devices either positively or negatively [1]. The formation energy and the transition charge state levels created in the band gap are important parameters that determine the effect of defect in a semiconductor [5]. Several experimental and theoretical studies of point defects such as vacancies and diffusion [6–9], interstitials [1,10] and impurity substitution [11,12] in Ge had been investigated using different techniques and approaches. The rare earth (RE) are good examples of elements that have amongst other orbitals, the *4f* orbital at the valence shell, which are highly localized [13,14]. The RE are mainly use to generate optical sources over extensive wavelength range from the visible to the infrared regions [15,16]. The optical properties of RE give a proper description of the photoluminescence experience in a RE related defect in Si [15]. Recently fabrication and optical properties of Tm doped materials were studied and electro-luminescence (EL) has been demonstrated from this material [17–19]. Light emission devices have been attributed to thulium and erbium defects in several materials [20,21]. For Ge, Tm^{3+} defects were extensively studied using a screened hybrid functional [11]. According to *Ref* [11], the Tm^{3+} interstitial and substitutional defects in Ge exist with low formation energies and Tm^{3+} defect introduced transition levels of $(0/-1)$, $(+1/0)$ and $(+1/+2)$ within the band gap [11]. Vacancy impurity complexes in Ge are important because many substitutional centres including dopant migrate by thermally generated vacancies [22]. The results of the RE defect related complexes in GaN [23–25], AlN/Si [26] and GaAs [27] has been previously studied and reported. It have been predicted that the RE defect complexes in GaN exhibit charge state controlled metastability [23]. While for Si, the RE impurities are electrically inert and induced gap levels occupied by the valence electrons [26], but for AlN, the RE impurities induced deep levels within the band gap [28]. For the GaN, AlN, GaAs and Si, the structural and electronic properties of the RE induced defects has been successfully predicted. However, the structural and

* Corresponding author. Department of Physics, University of Pretoria, Pretoria 0002, South Africa.
** Corresponding author.
E-mail addresses: elgumuk@gmail.com (E. Igumbor), wmeyer@up.ac.za (W.E. Meyer).

http://dx.doi.org/10.1016/j.cocom.2016.07.003

electronic properties of RE induced defect complexes in Ge have not been reported both experimentally and theoretically. In this work, we have used the screened hybrid functional of Heyd, Scuseria, and Ernzerhof (HSE06) [29] by means of density functional theory (DFT) to calculate the structural and electronic properties of the Tm^{3+}-V_{Ge} defect complexes in Ge for the nearest neighbour (*fnn*), second nearest neighbour (*snn*), third nearest neighbour (*tnn*) and fourth nearest neighbour ($f_t nn$) configurations. The energies of formation for the various configurations were calculated for charge states $(-2, -1, 0, +1, and +2)$. The charge states transition levels for the Tm^{3+}-V_{Ge} were examined and presented. The role of shallow levels and charge state controlled metastability along side with *negative-U* behaviour were also discussed. The remaining parts of this paper have been organised as follows: in Section 2, we present a description of the computational details, followed by the results and discussion in Section 3 and finally, we present our concluding remarks in Section 4.

2. Computational details

Using the Vienna *ab-initio* Simulation Package (VASP) [30,31], we have carried out DFT calculation of the Tm^{3+}-V_{Ge}. The inert core electrons were separated from the chemically active valence electrons by using the Projector-augmented wave (PAW) method, as implemented in the VASP code [30,32]. For Ge, the 4*s* and 4*p* electrons in the outer shell were treated as valence electrons, while for Tm^{3+}, the 6*s*, 5*p* and 4*f* orbitals were considered as valence electrons. DFT calculations were carried out using the HSE06 hybrid functional [29,33]. In this approach, the short-range exchange potential was calculated by mixing a fraction (25%) of nonlocal Hartree-Fock exchange with the generalized gradient approximation (GGA) functional of Perdew, Burke, and Ernzerhof (PBE) [34]. In contrast to the local density approximation and the generalized gradient approximation that underestimate the band gap of the semiconductor [35,36], the HSE06 functional gives an excellent description of the electronic band gap for a wide range of defects in group-IV semiconductors [37,10]. For the past decades, the study and prediction of the electronic properties of materials with the *4f* orbital valence electron was difficult due to the fact that the *f* orbital is highly localised. The highly localised *4f* orbital was previously treated using LDA + U and other methods [13,38–40]. Recently, the hybrid density functional has been successfully used to predict the electronic properties of several materials with highly localized *f* orbitals in the valence shell [13,14]. Following this success of the hybrid density functional, it became feasible to handle the *4f* orbital in the valence shell of Tm^{3+}. For the bulk, geometric optimization of Ge was performed in an 8-atom unit cell with an 8^3 Monkhorst-Pack [41] k-point Brillouin zone sampling scheme and cutoff energy of 400 eV. For the defects, we employed a 64 atom supercell using a 2^3 Monkhorst-Pack [41] k-point Brillouin zone sampling scheme, and we set the plane wave cutoff of the wave function expansion to 400 eV. We refined the structure until the change in the total energy was less than 10^{-5} eV and the forces were relaxed to below 0.001 eV/Å. In all the calculations, spin orbit coupling was taken into account To calculate the defect formation and transition energy $(\varepsilon(q/q'))$ levels, we calculated the total energy $E(d, q)$ for a supercell containing the optimized defect *d* in its charge state *q*. The defect formation energy $E^f(d, q)$ as a function of electron Fermi energy (ε_F) relative to the valence band edge is given as [42,43].

$$E^f(d,q) = E(d,q) - E(pure) + \sum_i (\Delta n)_i \mu_i + q[E_V + \varepsilon_F] + E^q_{cor}, \tag{1}$$

where $E(pure)$ is the energy of a supercell without a defect, $(\Delta n)_i$ is the difference in the number of constituent atoms of type *i* between the pristine and the supercell containing the defect, μ_i represents the chemical potential of different constituent atoms and E_V is the valence band maximum (VBM). Errors in $E^f(d, q)$ due to finite-size effects within the supercell and inaccuracy underlying the approximation of the energies, were handled by including the correction E^q_{cor} term according to FNV [43,44]. The defect transition energy level $\varepsilon(q/q')$ is the Fermi energy at which two charge states (q and q') of the defect have the same energy of formation is given as [5].

$$\varepsilon(q/q') = \frac{E^f(d,q;\varepsilon_F = 0) - E^f(d,q';\varepsilon_F = 0)}{q' - q} \tag{2}$$

As reported in Ref. [10], we took the modelled band gap of the pristine Ge at 0 K to be 0.78 eV. The binding energies E_b which are defined as the energy required to split up defect cluster into well separated non-interacting defects is given as [45].

$$E_b = E^f_{V_{Ge}} + E^f_{Tm^{3+}_{Ge}} - E^f_{defect-complex}, \tag{3}$$

where $E^f_{V_{Ge}}$, $E^f_{Tm^{3+}_{Ge}}$ and $E^f_{defect-complex}$ are the formation energies of V_{Ge}, Tm^{3+}_{Ge} and Tm^{3+}-V_{Ge} respectively. Eq. (3) could be interpreted as the energy loss of the bonded structure with respect to the isolated components.

3. Results and discussion

3.1. Structural properties of Tm^{3+}-V_{Ge}

The geometric structures of Tm^{3+}-V_{Ge} for four configurations are shown in Fig. 1. Fig. 1a and b show the relaxed geometric structure of the first nearest neighbour (*fnn*) and second nearest neighbour (*snn*), respectively. While Fig. 1c shows the relaxed geometric structure of the third nearest neighbour (*tnn*), Fig. 1d displays the relaxed geometric structure of the fourth nearest neighbour ($f_t nn$). Fig. 1e is the extract of the Tm atom with its four nearest neighbour Ge atoms. For the *fnn* configuration, the Tm-Ge bond length decreased by 0.01 Å. Whereas two bond angles formed decreased by 1° and the other two bond angles were unchanged. For the *snn* configuration, we observed that the Tm-Ge bond length decreased by 0.5 and 0.10 Å except for in one direction, where the bond length increased by 0.40 Å. For the bond angle in *snn* configuration, while two bond angles decreased by 8° and 10°, the other 2 bond angles increased by 7° and 10°. For the *tnn* configuration, all the optimised bond length increased by an average of 0.40 Å and half of the bond angles formed increased by 7° and 1°, while the other half decreased by 8° and 2°. Finally for the $f_t nn$ configuration, all the bond length increased by an average of 0.28 Å. The bond angles formed increased by 2° and 9° except for in one, which decreased by 8°.

3.2. Formation energies and thermodynamic properties of Tm^{3+}-V_{Ge}

Results of the formation energies of Tm^{3+}-V_{Ge} in its various configurations are tabulated in Table 1. In all the configurations, the defect Tm^{3+}-V_{Ge} forms with formation energies between 4.00 and 7.50 eV. Under equilibrium conditions, the *fnn* configuration is energetically more favourable in all charge states except for the − charge state where the $f_t nn$ is energetically most favourable. The Tm^{3+}-V_{Ge} had a lower formation energy in the *tnn* configuration than the *snn* configuration. In the neutral state, the energy difference between the *fnn* and the *snn* is 2.01 eV. By using Eq. (3), we

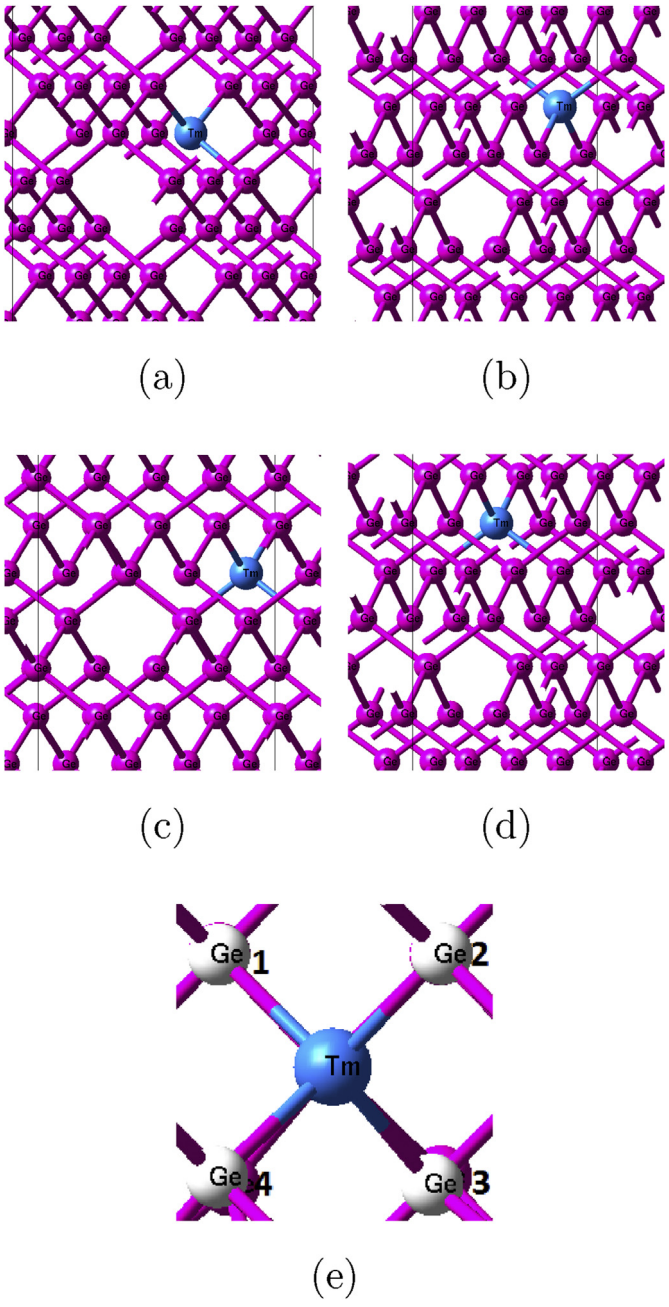

Fig. 1. Geometric structure of the Tm^{3+}_{Ge}-V_{Ge} complex in Ge for the (a) first nearest neighbour, (b) second nearest neighbour, (c) third nearest neighbour, (d) fourth nearest neighbour and (e) extract of the Tm and its nearest neighbour Ge atoms.

Table 1
Calculated formation energies (E^f) in eV at $\varepsilon_f = 0$ of Tm^{3+}_{Ge}-V_{Ge} complexes in Ge for the first nearest neighbour (*fnn*), second nearest neighbour (*snn*), third (*tnn*) nearest neighbours and the fourth (f_t *nn*) configurations. The lowest formation energy in each charge state are written in bold.

Defect	Configuration	−2	−1	0	+1	+2
Tm^{3+}_{Ge}−V_{Ge}	*fnn*	**4.78**	4.72	**5.06**	**4.88**	**5.17**
	snn	6.54	8.79	7.07	7.30	7.64
	tnn	6.01	5.60	5.17	5.12	5.55
	f_t *nn*	4.88	**4.67**	5.07	5.69	5.90

calculated the binding energies for the Tm^{3+}-V_{Ge} in the neutral state to be 0.06, −0.05, − 1.95 and 0.05 eV for the *fnn*, *snn*, *tnn* and the f_t*nn* configurations, respectively. The binding energies suggest that the *fnn* and f_t*nn* configurations can form without dissociating.

Table 2
The energy of the charge state transition levels $\varepsilon(q/q')$ above E_V (eV) for the *fnn*, *tnn* and f_t *nn* configurations of Tm^{3+}_{Ge}-V_{Ge} complexes.

Charge states	*fnn*	*tnn*	f_t *nn*
(+1/0)	–	0.05	–
(0/−2)	–	0.41	–
(−1/−2)	0.06	–	0.21

The plot of the charge state transition levels for the *fnn*, *snn*, *tnn* and f_t*nn* configurations of Tm^{3+}-V_{Ge} are presented in Fig. 2. Fig. 2a and d show the plot of the formation energies of Tm^{3+}-V_{Ge} in its charge states as a function of ε_F for the *fnn*, *snn*, *tnn* and f_t*nn* configurations respectively. Fig. 2e represents the thermodynamically most stable accessible region for the *fnn*, *snn tnn* and f_t*nn* configurations. Table 2 lists the energy of the charge state transition levels. For the *fnn* configuration, the Tm^{3+}-V_{Ge} induced a double shallow acceptor level at E_V + 0.06 eV close to the valence band maximum (VBM). There was no other thermodynamically accessible induced level found for the *fnn* configurations. For the *snn* configurations, there was no transition level induced by Tm^{3+}-V_{Ge} within the band gap. The −2 charge state has the lowest energy level across the band gap. This is in contrast to the *tnn* configuration where we observed the presence of two levels within the band gap. These levels are single donor, located at E_V + 0.05 eV and an acceptor deep level at E_V + 0.41 eV. All other possible transition levels are at almost 1 eV away from the stable region within the band gap. For the f_t*nn* configuration, we observed a single Tm^{3+}-V_{Ge} induced level. Quite interestingly, the level is a shallow acceptor at E_V + 0.16 eV close to the VBM. For all the observed induced levels within the band gap, we discovered that the Tm^{3+}-V_{Ge} is most likely to form acceptor levels than donor levels and most of these levels are close to the VBM.

The Tm^{3+}-V_{Ge} induced defect in Ge reveals interesting properties, such as the charge state controlled metastability and the *negative-U* properties. In Fig. 2e, for the *fnn* and f_t*nn* configurations we noticed the evidence of charged state controlled metastability. The implication of the presence of charge state controlled metastability is that the minimum energy configuration of the Tm^{3+}-V_{Ge} can be controlled by changing the charged state of the defect from −1 to −2. The difference in energy between the *fnn* and f_t*nn* configurations for charge state −1 and −2 is small (0.05 and 0.1 eV respectively). This difference is in order of K_B T at room temperature, so both states should be occupied at room temperature. Taking the high energy of formation of the *snn* and *tnn* configurations, it seems there is a large energy barrier between the two states. In addition, the low binding energy of the defect makes it unlikely for vacancies to be captured for long. It is therefore doubtful if there will be enough opportunity for a significant number of vacancies in the f_t*nn* configuration to surmount the barrier in order for the defect to transform to its *fnn* states. While there was no evidence of *negative-U* behaviour for the *fnn* and f_t*nn* configurations, in the *tnn* configurations, the Tm^{3+}-V_{Ge} exhibited the properties of *negative-U* with *effective-U* value of −0.42 eV. The Tm^{3+}-V_{Ge} complexes enhance the efficient ionization of electrons from the valence band which in turn create holes in the valence band. The Tm^{3+} defects in Ge should be used to control conductivity since it exhibit the properties of shallow levels.

4. Conclusion

In conclusion, the density function theory (DFT) with the screened Heyd, Scuseria, and Ernzerhof (HSE06) hybrid function

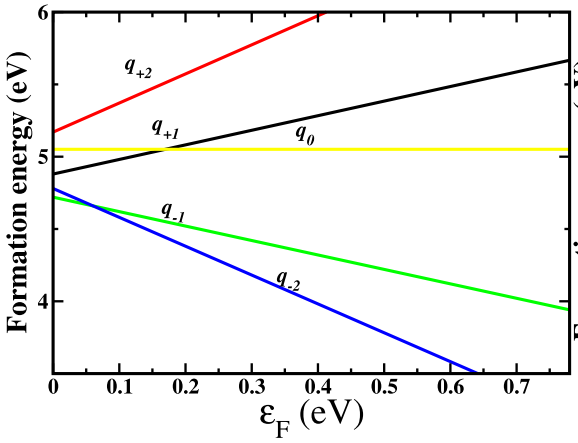

(a) First nearest neighbour (*fnn*).

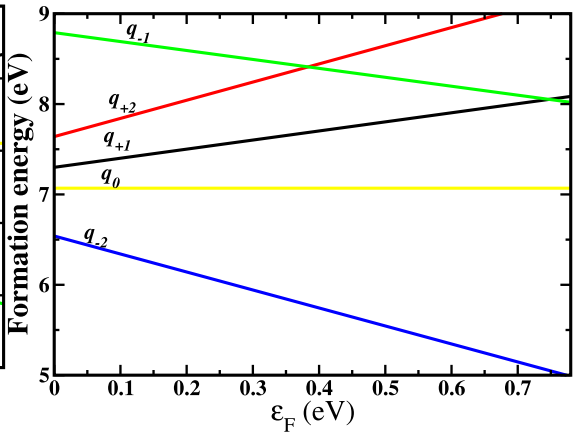

(b) Second nearest neighbour (*snn*).

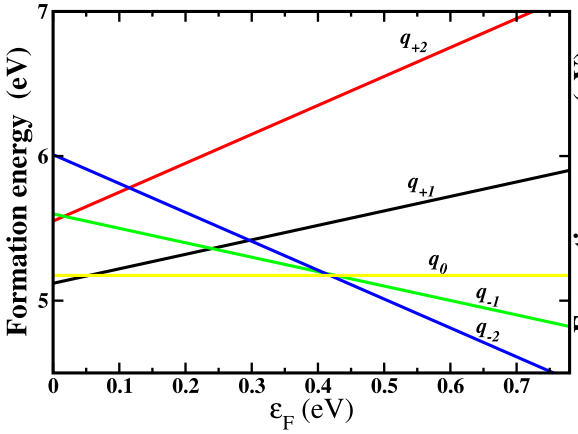

(c) Third nearest neighbour (*tnn*).

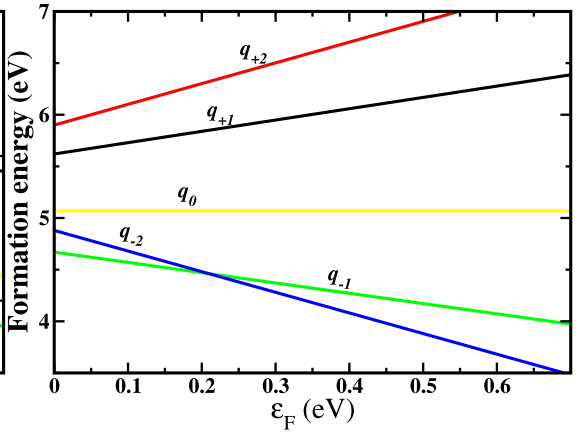

(d) Fourth nearest neighbour ($f_t nn$).

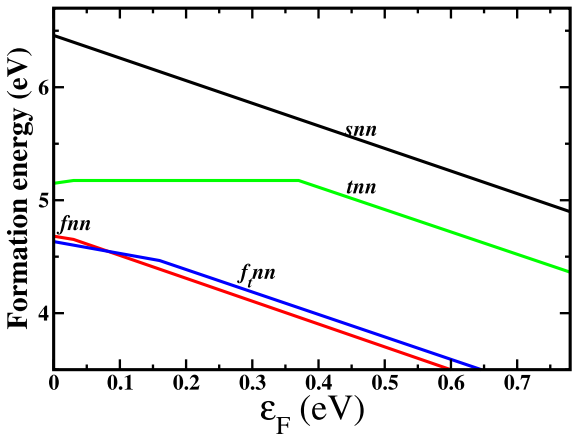

(e) Thermodynamically stable region for various configurations.

Fig. 2. Plot of formation energy as a function of the Fermi energy of the Tm^{3+}_{Ge}-V_{Ge} complexes in Ge for the *fnn*, *snn*, *tnn* and *ft nn* configurations. Fig. 2e shows the most thermodynamically stable region within the band gap for the various configurations being examined. The *fnn* and $f_t nn$ configurations displayed the properties of charged state controlled metastability and the *tnn* displays *negative-U* properties.

were used to calculate the Tm^{3+}-V_{Ge} in its four different configurations (first nearest neighbour (*fnn*) second nearest neighbour (*snn*), third nearest neighbour (*tnn*) and the fourth nearest neighbour ($f_t nn$). The structural properties, electronic properties, formation energies and charge state thermodynamic transition levels were calculated and described. We have shown that the

formation of the Tm^{3+}-V_{Ge} occurred in four different configuration with low formation energy except for the *snn* configuration which had a high formation energy. The *fnn* and $f_t nn$ configurations of the Tm^{3+}-V_{Ge} defect under equilibrium condition were energetically most favourable. For the neutral state the *fnn* and $f_t nn$ forms with 5.06 and 5.07 eV formation energies and with a positive binding energy of 0.06 and 0.05 eV respectively. The charge state transition levels shown that the Tm^{3+}-V_{Ge} induced shallow levels close to the valence band maximum. These shallow levels are acceptor at $\varepsilon(-1/-2) = 0.06$ eV and $\varepsilon(-1/-2) = 0.21$ eV for the *fnn* and $f_t nn$ configurations respectively and donor at $\varepsilon(+1/0) = 0.05$ eV for the *tnn* configuration. In addition, Tm^{3+}-V_{Ge} displayed the properties of charge state controlled metastability between the *fnn* and the $f_t nn$ configurations. We have pointed out the role of vacancy complexes in Ge and we expect the data and information presented to be useful in the process modelling of Ge-based devices for industrial applications.

Acknowledgement

This work is based on the research supported partly by National Research foundation (NRF) of South Africa (Grant specific unique reference number (UID) 78838). The opinions, findings and conclusion expressed are those of the authors and the NRF accepts no liability whatsoever in this regard.

References

[1] C. Claeys, E. Simoen, Germanium-based Technologies: from Materials to Devices, Elsevier, 2011.
[2] O. Madelung, Semiconductors Basic Data, Springer Science & Business Media, 2012.
[3] F.J. Morin, J.P. Maita, Phys. Rev. 94 (1954) 1525–1529.
[4] L. Lee, E.A. Fitzgerald, T. Bulsara, Mayank T. Currie, A. Lochtefeld, J. Appl. Phys. 97 (1) (2005) 011101.
[5] Christoph Freysoldt, Blazej Grabowski, Tilmann Hickel, J. Neugebauer, Georg Kresse, Anderson Janotti, C.G.V. de Walle, Rev. Mod. Phys. 86 (2014) 253–305.
[6] S. Coelho, F. Auret, P.J. van Rensburg, J. Nel, Phys. B Condens. Matter 439 (0) (2014) 97–100.
[7] R. Kube, H. Bracht, A. Chroneos, M. Posselt, B. Schmidt, J. Appl. Phys. 106 (6) (2009) 063534.
[8] A. Chroneos, H. Bracht, Diffusion of n-type dopants in germanium, Appl. Phys. Rev. 1 (1) (2014) 011301.
[9] H. Tahini, A. Chroneos, R. Grimes, U. Schwingenschlögl, Appl. Phys. Lett. 99 (16) (2011) 162103.
[10] E. Igumbor, C.N.M. Ouma, G. Webb, W.E. Meyer, Phys. B Condens. Matter 480 (2016) 191–195.
[11] E. Igumbor, W.E. Meyer, Mater. Sci. Semicond. Process. 43 (2016) 129–133.
[12] J. Lauwaert, S. Segers, F. Moens, K. Opsomer, P. Clauws, F. Callens, E. Simoen, H. Vrielinck, J. Phys. D Appl. Phys. 48 (17) (2015) 175101.
[13] B.G. Janesko, T.M. Henderson, G.E. Scuseria, Phys. Chem. Chem. Phys. 11 (3) (2009) 443–454.
[14] J.L. Da Silva, M.V. Ganduglia-Pirovano, J. Sauer, V. Bayer, G. Kresse, Phys. Rev. B 75 (4) (2007) 045121.
[15] J.H. Castilho, I. Chambouleyron, F.C. Marques, C. Rettori, F. Alvarez, Phys. Rev. B 43 (11) (1991) 8946.
[16] A.G. Raffa, P. Ballone, Phys. Rev. B 65 (12) (2002) 121309.
[17] F. Fang, A. Ng, X. Chen, A. Djurii, Y. Zhong, K. Wong, P. Fong, H. Lui, C. Surya, W. Chan, Mater. Chem. Phys. 125 (3) (2011) 813–817.
[18] M. Peres, J. Wang, M. Soares, A. Neves, T. Monteiro, E. Rita, U. Wahl, J. Correia, E. Alves, Superlattices Microstruct. 36 (46) (2004) 747–753.
[19] T. Monteiro, A. Neves, M. Soares, M. Carmo, M. Peres, E. Alves, E. Rita, Appl. Phys. Lett. 87 (19) (2005) 192108.
[20] M. Lourenço, C. Opoku, R. Gwilliam, K. Homewood, Opt. Mater. 32 (12) (2010) 1597–1600.
[21] A. Polman, J. Appl. Phys. 82 (1) (1997) 1–39.
[22] J. Coutinho, S. Öberg, V.J.B. Torres, M. Barroso, R. Jones, P.R. Briddon, Phys. Rev. B 73 (2006) 235213.
[23] C.N. Ouma, W.E. Meyer, Phys. B Condens. Matter 439 (2014) 141–143.
[24] S. Sanna, W. Schmidt, T. Frauenheim, U. Gerstmann, Phys. Rev. B 80 (10) (2009) 104120.
[25] J.-S. Filhol, R. Jones, M. Shaw, P. Briddon, Appl. Phys. Lett. 84 (15) (2004) 2841–2843.
[26] R. Jones, Opt. Mater. 28 (6) (2006) 718–722.
[27] A. Svane, N.E. Christensen, L. Petit, Z. Szotek, W. Temmerman, Phys. Rev. B 74 (16) (2006) 165204.
[28] S. Wang, X. Wang, J. Li, Y. Jia, F. Wang, Mod. Phys. Lett. B 29 (21) (2015) 1550114.
[29] J. Heyd, G.E. Scuseria, M. Ernzerhof, J. Chem. Phys. 118 (18) (2003) 8207–8215.
[30] G. Kresse, J. Furthmüller, Phys. Rev. B 54 (1996) 11169–11186.
[31] G. Kresse, D. Joubert, Phys. Rev. B 59 (1999) 1758–1775.
[32] P.E. Blochl, Phys. Rev. B 50 (1994) 17953–17979.
[33] J. Heyd, G.E. Scuseria, J. Chem. Phys. 120 (16) (2004) 7274–7280.
[34] J.P. Perdew, K. Burke, M. Ernzerhof, Phys. Rev. Lett. 77 (1996) 3865–3868.
[35] H. Tahini, A. Chroneos, R. Grimes, U. Schwingenschlögl, H. Bracht, Appl. Phys. Lett. 99 (7) (2011) 072112.
[36] P. Śpiewak, J. Vanhellemont, K. Sueoka, K. Kurzydłowski, I. Romandic, Mater. Sci. Semicond. Process. 11 (5) (2008) 328–331.
[37] P. Deák, B. Aradi, T. Frauenheim, E. Janzén, A. Gali, Phys. Rev. B 81 (2010) 153203.
[38] V.I. Anisimov, J. Zaanen, O.K. Andersen, Phys. Rev. B 44 (3) (1991) 943.
[39] L. Petit, A. Svane, Z. Szotek, W.M. Temmerman, Phys. Rev. B 72 (20) (2005) 205118.
[40] M. Cococcioni, S. De Gironcoli, Phys. Rev. B 71 (3) (2005) 035105.
[41] H.J. Monkhorst, J.D. Pack, Phys. Rev. B 13 (1976) 5188–5192.
[42] S.B. Zhang, J.E. Northrup, Phys. Rev. Lett. 67 (1991) 2339–2342.
[43] C. Freysoldt, J. Neugebauer, C.G. Van de Walle, Phys. Status Solidi (b) 248 (5) (2011) 1067–1076.
[44] Y. Kumagai, F. Oba, Phys. Rev. B 89 (2014) 195205.
[45] G. Zollo, Y.J. Lee, R.M. Nieminen, J. Phys. Condens. Matter 16 (49) (2004) 8991.